Gas breakdown in atmospheric pressure microgaps with a surface protrusion on the cathode

Yangyang Fu,[1,2,a)] Peng Zhang,[2] and John P. Verboncoeur[1,2]
[1]*Department of Computational Mathematics, Science and Engineering, Michigan State University, East Lansing, Michigan 48824, USA*
[2]*Department of Electrical and Computer Engineering, Michigan State University, East Lansing, Michigan 48824, USA*

(Received 26 April 2018; accepted 6 June 2018; published online 21 June 2018)

Gas breakdown in atmospheric pressure microgaps with a cathode surface protrusion is highly sensitive to the protrusion geometry. The breakdown voltage is identified when the discharge enters the subnormal region, according to voltage-current curves calculated by a two-dimensional fluid model. The effects of the protrusion size and the aspect ratio on the gap breakdown voltage are examined. It is found that the protrusion size can have a more profound effect on the breakdown voltage than the protrusion's aspect ratio. The breakdown voltage versus the protrusion aspect ratio will show a minimum value if the aspect ratio varies in a wider range. Shrinking the size of cathode protrusion can increase the breakdown voltage faster than enlarging the gap distance in the absence of a protrusion in the same scale. The effect of the aspect ratio of the microgap on the breakdown voltage is also presented. *Published by AIP Publishing.* https://doi.org/10.1063/1.5037688

In recent years, microplasmas and microdischarges with characteristic lengths less than 1 mm have received growing attention because of their various prospective applications, including plasma display panels, ion sources, micro-electro-mechanical systems, micro-switches, and microchip devices.[1–5] With the rise of 3D printing capabilities, the fabrication technology enables increasingly complicated geometries in plasma devices down to the micron scale.[6,7] However, controlling the surface finish of electrodes is difficult in micro-systems and absolutely smooth surfaces would maximize voltage hold-off. Even if this finish could be achieved during fabrication, surface roughening may still be introduced from "scratch-and-dig" during handling and assembly or from sputtering, micro-arcs and deposition, where surface features are created. Since at high pressure the discharge dimensions are sharply reduced with the *pd* scaling, gas breakdown characteristics can be more complex when the presence of a surface protrusion on the electrode becomes important.[8–11]

Recent studies distinguished the microdischarges driven by different emission mechanisms. For a direct-current (DC) microdischarge, it is ignited and maintained by secondary electron emission when the gap distance is greater than $\sim$10 μm, while the dominant mechanism becomes electron field emission when the gap distance is less than a few microns, especially with microprotrusions on the cathode surface.[12–14] The presence of the protrusion on the electrode surface usually leads to enhancement of the local electric field.[15] When the electric field at the cathode surface reaches the order of 10^9 V/m, field emission starts to play a key role.[16–19] A comprehensive analysis on the field distribution and the current emission in the presence of a sharp protrusion in a finite cathode-anode gap was given by Zhang *et al.*[20,21] However, under certain conditions, the presence of the surface protrusion does not necessarily bring the discharge into the regime with field emission. Levko and Raja employed a fluid model of a xenon microdischarge at 10 atm with a hemispherical protrusion on both anode and cathode and found that the discharge is mainly sustained by the secondary electron emission on the cathode.[22] For normal atmospheric discharges, the electric field is of the order of 10^7 V/m, for which the presence of surface protrusions with a smooth tip, though leading to electric field enhancement, will not necessarily result in significant field emission. With a hemispherical protrusion on the cathode, the enhanced electrostatic field is only about 3 times the average field.[23] Depending on the protrusion geometry, the field enhancement can be either strong or weak and its impact on the discharge properties varies.[24] Despite extensive studies of microdischarges, the effects of surface protrusions on the gas breakdown characteristics have only been investigated under limited discharge conditions.

This letter focuses on the impact of the cathode current emission enhancement caused by a smooth-tip electrode protrusion on the gas breakdown characteristics. Unlike the slow glow breakdowns or the streamer breakdowns in other situations, here gas breakdown with a cathode surface protrusion mainly occurs in the transition between the Townsend discharge regime and the subnormal glow discharge regime. With a hemi-ellipsoidal protrusion on the cathode surface, the breakdown voltage was quantified based on the voltage-current (V-I) characteristics using a two-dimensional fluid model. By adjusting the protrusion geometry, the effects of the size and the aspect ratio of the surface protrusion on the breakdown voltage and the cathode current emission were studied. The effect of the microgap aspect ratio (the gap length over the electrode radius) on the breakdown voltage was also examined.

The schematic of the microgap is shown in Fig. 1. The microgap consists of two plane-parallel circular electrodes

[a)]Author to whom correspondence should be addressed: fuyangya@egr.msu.edu

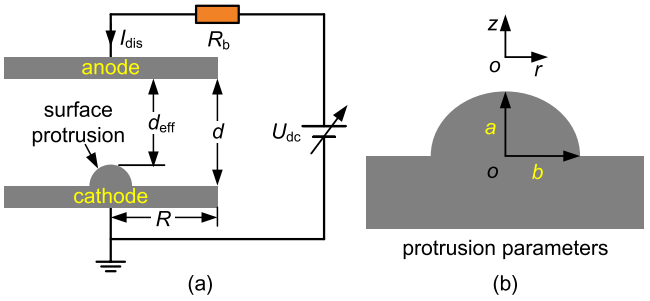

FIG. 1. Schematic of the microdischarges. (a) The microgap with a DC voltage source U_{dc} applied through a ballast resistor R_b while the cathode is grounded and (b) protrusion parameters: a is the axial dimension and b is the radial dimension.

with a single hemi-ellipsoidal cathode protrusion. A DC voltage is applied to the anode through a ballast resistor R_b, while the cathode is grounded, as shown in Fig. 1(a). The parameter d is the gap length, R is the electrode radius, and d_{eff} is the effective (or minimum) gap distance, which is the length between the anode and the protrusion tip. The parameters a and b are used to define the geometry of the hemi-ellipsoidal protrusion, as shown in Fig. 1(b). The aspect ratio a/b reflects the sharpness of the geometry shape. The coordinate is in the r–z plane, and the protrusion height a varies in the range of 25–100 μm.

The two-dimensional fluid model consists of a set of coupled equations, including the species continuity equations, electron energy conservation equation, and Poisson's equation.[25–27] The detailed description of the fluid model can be found in previous studies, and a short description is provided here for convenience.[28,29] Argon gas at room temperature 300 K (0.026 eV) and one atmosphere is chosen as the working gas. In the cases studied, since the magnitude of the cathode electric field (10^6–10^7 V/m) is much less than the field emission threshold ($\sim 10^9$ V/m or larger), field emission is ignored and the discharge is sustained by ion-impact secondary electron emission at the cathode.[12–14] The normal flux of electrons emitted by the cathode is related to the flux of incident ions by an effective secondary emission coefficient γ, which is fixed at 0.1.[30,31] The equations of the discharge model are solved self-consistently to steady-state.

The voltage-current characteristic identifies the operating regime of the discharge. By increasing the applied voltage U_{dc} gradually at small intervals in a sequence of simulations, a typical representation of the relationships between the applied voltage U_{dc}, gap voltage U_{gap}, and the discharge current I_{dis} is obtained, as shown in Fig. 2(a). It can be seen that the V-I curve is composed of three regimes, i.e., Geiger-Müller (G-M) regime, Townsend discharge regime, and subnormal glow discharge regime, which are delimited by current intervals. The G-M regime was historically used to measure the intensity of nuclear radiation, and the discharge current can be as low as 10^{-16} A.[32] In this regime, as the applied voltage increases, the free charge physically contributed by random sources (such as cosmic radiations) can be absorbed by the electrodes, reaching a saturation point. In the Townsend regime, the gap voltage is roughly constant, while with a slight increase in the applied voltage, the discharge current increases by several orders of

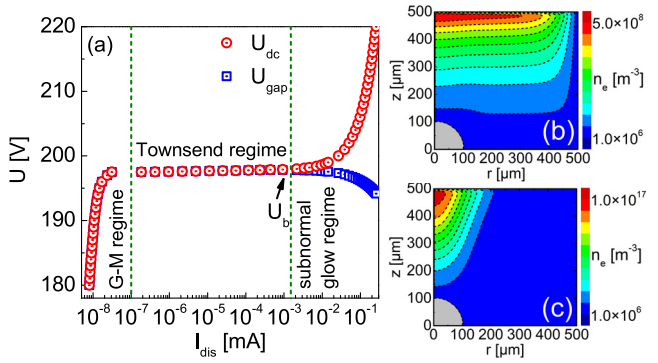

FIG. 2. (a) The voltage-current characteristics for an atmospheric microgap with a cathode surface protrusion ($a = b = 100$ μm) and the electron density distributions in (b) the G-M regime, and (c) the Townsend regime. In the simulation, we set $R = 500$ μm and $d = 500$ μm.

magnitude. As the applied voltage further increases, the V-I curve reaches a critical point, which is referred as the breakdown point, where the discharge enters the subnormal glow regime, showing a negative differential resistance behavior. The applied voltage was swept with sufficiently small steps to capture the V-I curve across different regimes. Figures 2(b) and 2(c) show the electron density distribution in the G-M and the Townsend regimes, respectively. In the G-M regime, the electron density is only of the order of 10^8 m^{-3} and the gradient of the density is relatively flat in the radial direction. When the discharge reaches the Townsend breakdown point, the electron density has an order of 10^{17} m^{-3}, which is typical for the atmospheric Townsend discharges or the early stage of subnormal glow discharges. The discharge current is still relatively small, the space charge has little influence, and the cathode sheath have not developed yet.[32] According to the obtained V-I curve, the breakdown voltage can be identified with an uncertainty less than 0.5 V without alternative criteria.

The effects of the protrusion aspect ratio and size on the breakdown voltages are shown in Fig. 3. In Fig. 3(a), when the protrusion is hemispherical ($a = b$), as the protrusion size increases from 25 to 100 μm, the breakdown voltage decreases from 220 to 197 V. When the axial dimension a is fixed at 100 μm and the radial dimension b decreases from 200 to 50 μm, with the aspect ratio a/b increasing from 0.5 to 2.0, the breakdown voltage is found with little changes, from

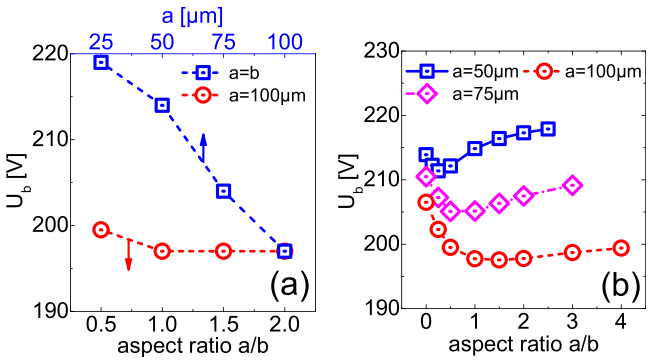

FIG. 3. (a) Comparing the effects of protrusion size and aspect ratio on breakdown voltages in microgaps and (b) the breakdown voltage versus the aspect ratio with different protrusion heights. In the simulation, we set $R = 500$ μm and $d = 500$ μm.

200 to 197 V. The breakdown voltage is more sensitive to the protrusion size than the aspect ratio. This can be explained directly based on the self-sustained condition for Townsend discharges.

The criterion for Townsend breakdown is expressed as

$$\int_0^d \alpha(z) \cdot \mathrm{d}z \geq \ln(1 + 1/\gamma), \tag{1}$$

where $\alpha(z)$ is the electron impact ionization coefficient and is a function of the reduced electric field E/p.[33] For rare gases, $\alpha(z)$ can be expressed as

$$\alpha(z) = \mathrm{A} \cdot p \cdot \exp\left[-\mathrm{B}/\sqrt{E(z)/p}\right], \tag{2}$$

where p is the gas pressure, and A and B are fitted constants. Equation (1) means that for breaking down a gaseous gap, it is necessary to produce a sufficiently large number of ionizations by electron avalanches to self-sustain the discharge.[35] With the same field enhancement but a shorter effective distance d_{eff}, the breakdown voltage is expected to be lower when the protrusion size on the cathode is larger, since according to Eq. (2), the ionization coefficient increases exponentially with $\sqrt{E(z)/p} \sim \sqrt{U/d_{\mathrm{eff}}}$. This is indeed the case, as shown in Fig. 3(a) for the case of $a = b$. On the other hand, with the same protrusion height but different radial dimensions, as the aspect ratio a/b increases, the electric field enhancement as well as the local ionization coefficient increases. Hence, with a larger aspect ratio, the breakdown voltage is supposed to be lower since the ionizations are enhanced and become more effective. However, only a slight drop of the applied voltage is observed in Fig. 3(a) for the case of $a = 100\,\mu$m. In order to examine the effect of the aspect ratio in a wider range, we carried out the simulations with more designed cases. In Fig. 3(b), breakdown voltages were obtained with a fixed at 50, 75, and 100 μm, respectively, and the aspect ratio varies in a wider range, from 0 to 4.0. For a given a, the breakdown voltage as a function of the aspect ratio shows a minimum, being a V-shaped curve. The result reveals that the aspect ratio does not necessarily have a monotonic impact on the breakdown voltage. This behavior is very different from the expectation that the breakdown voltage will decrease if the protrusion becomes sharper. In the following, the emitted current density distributions on the cathode are investigated to find the reason for this.

Figure 4 shows the characteristics of the current emission on the cathode. In all the cases, the protrusion height a is fixed at 100 μm. The cathode current enhancement is investigated with the radial dimension b ranging from 25 to 400 μm, corresponding to the aspect ratio in the range of 0.25–4. In Fig. 4(a), the maximum current density $J_{\mathrm{max}} = J(0)$ is normalized with the averaged current density $J_{\mathrm{av}} = I_{\mathrm{dis}}/S_{\mathrm{cathode}}$, where I_{dis} is the total discharge current and S_{cathode} is the total cathode surface area. It is observed that the current density enhancement $J_{\mathrm{max}}/J_{\mathrm{av}}$ increases before reaching breakdown. Also, the larger the protrusion aspect ratio, the larger the current enhancement. When the applied voltage reaches the breakdown voltage, the current density enhancement reaches a maximum point, and after the breakdown point, it remains almost constant. The breakdown voltages shown in Fig. 4(a) are the same as those identified from the V-I curve in Fig. 2(a). In Fig. 4(a), taking the cases of a/b equals 1/4, 1.0, and 4.0, for example, the breakdown voltage drops first and then increases, which is also consistent with the result in Fig. 3(b). Figure 4(b) shows the spatial distribution of the normalized surface current density in the radial direction, at applied voltage of 205 V. It can be seen that in all cases the current density drops orders of magnitude at the protrusion boundary, i.e., $r/R = 0.05$, 0.1, 0.2, 0.4, 0.6, and 0.8, and have a small rebound outwards. The current density distribution profile is distorted and becomes zero at the corner between the protrusion and the substrate. The current density is enhanced at the protrusion surface but becomes relatively small (orders lower)

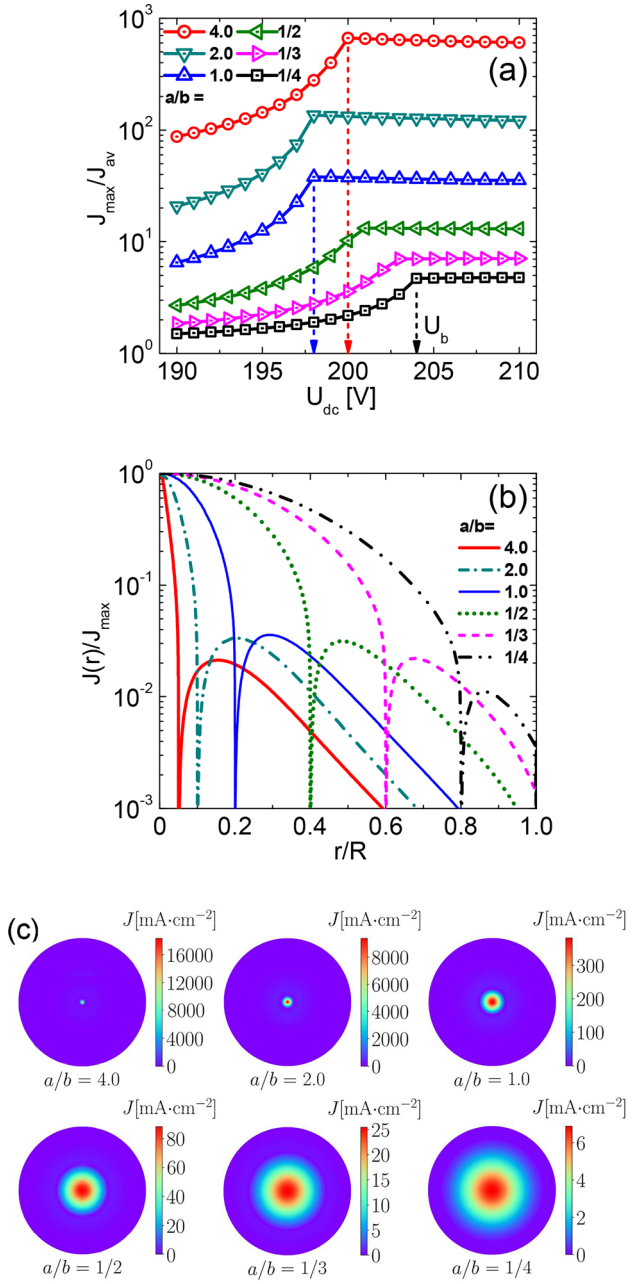

FIG. 4. Characteristics of the cathode current density with different protrusions of which the protrusion height a is fixed at 100 μm and the aspect ratio a/b ranges from 1/4 to 4.0. (a) The maximum current density J_{max} over the averaged current density J_{av} against the applied voltage U_{dc}; (b) the normalized current density distributions $J(r)/J_{\mathrm{max}}$ along the radial direction; and (c) the two-dimensional cathode surface current density distributions with the applied voltage $U_{\mathrm{dc}} = 205$ V.

elsewhere on the cathode. The general effect is that with a surface protrusion, the effective emission area decreases while the current magnitude is enhanced in the center.

The two-dimensional current density distribution on the cathode surface with the applied voltage of 205 V is shown in Fig. 4(c), where the effective emission area is inversely proportional to the current enhancement. Comparing the cases of the a/b equals to 4.0 and 1.0 in Fig. 4(c), even though the maximum current density for $a/b = 4.0$ is much larger than that for $a/b = 1.0$, the total current for the case of $a/b = 4.0$ is 6.02×10^{-2} mA, which is smaller than the total current of 8.62×10^{-2} mA for the case of $a/b = 1.0$. Therefore, a sharper protrusion will not necessarily increase the total discharge current since the current density enhancement competes with the effective emission area under different conditions. That is, a sharper protrusion will not necessarily lower the breakdown voltage. This explains the right branch of the breakdown curves in Fig. 3(b). As the aspect ratio increases, though achieved with a higher current density on the tip, the effective area decreases and the discharge requires a higher voltage to increase ionization frequency and a larger discharge current to ignite the breakdown.

In the cases studied above, the microgap's axial and radial dimensions are fixed, i.e., $d = R = 500\ \mu$m, keeping the aspect ratio $d/R = 1.0$. In Fig. 5(a), the effect of the microgap's aspect ratio on the breakdown voltage is presented. The gap distance d is fixed at 500 μm, and the radial dimension R ranges from 200 to 1000 μm, with the corresponding aspect ratio d/R varying from 0.5 to 2.5. With and without a hemispherical protrusion, the breakdown voltage increases significantly as d/R increases from 1.0 to 2.5 while remains a constant when $d/R \leq 1.0$. This shows that for both cases the smaller the electrode radius the higher the breakdown voltage, and the breakdown voltage saturates as the gap aspect ratio d/R becomes smaller than 1.0. This is due to radial diffusion of the charged particles and the similar behaviors of the aspect ratio d/R in low-pressure discharges are illustrated in Ref. 34. For a cylindrical column with radius R, the loss rate coefficient k_{loss} of transverse diffusion is inversely proportional to the square of the radius R, i.e., $k_{loss} \propto D_a \cdot (\chi_{01}/R)^2$, where $\chi_{01} = 2.405$ is the first zero of the Bessel function of zero order and D_a is the ambipolar diffusion coefficient.[35] In a microgap with a smaller radius, the radial loss rate coefficient is higher and the radial diffusion loss of the charged particles is more significant; thus, a higher breakdown voltage is needed to increase ionization and compensate the radial loss. As the radial dimension increases, the transverse diffusion loss becomes saturated and the breakdown voltage remains the same. This is so for gaps with and without a surface protrusion on the cathode. In Fig. 5(b), the breakdown voltage is shown as a function of the effective distance d_{eff} and the gap distance d, respectively, for a fixed $d/R = 1.0$. As the gap distance d increases, the breakdown voltage increases linearly with and without the hemispherical protrusion, where the slopes are nearly the same. When the gap distance d is fixed, by decreasing the protrusion size, the breakdown voltage, a function of effective distance d_{eff}, increases with a larger slope. Note that the effect of the aspect ratio on the breakdown voltage could be excluded since $d/R \leq 1.0$ is satisfied. The results indicate that, as compared to changing the gap distance d, changing the protrusion's size can adjust the breakdown voltage more efficiently, within a limited dimension.

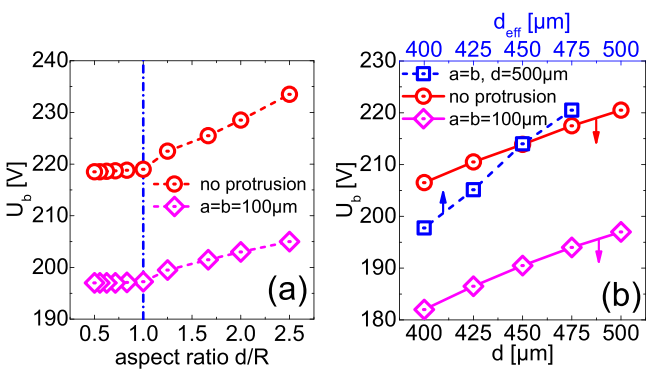

FIG. 5. (a) The effect of the microgap's aspect ratio d/R on the breakdown voltage in the microgap, with the gap distance d is fixed at 500 μm and the gap radius R increasing from 200 to 1000 μm, the aspect ratio ranging from 0.4 to 2.0 and (b) the breakdown voltage as a function of the effective distance d_{eff} and the gap distance d, for a fixed $d/R = 1.0$.

In summary, the gas breakdown in microgaps at atmospheric pressure with the presence of a cathode protrusion has been investigated. Based on the V-I curve calculated by a two-dimensional fluid model, the breakdown voltage is identified when the discharges go through the Townsend discharge region and enter into the subnormal glow region. The presence of the cathode protrusion will enhance the current density on the tip while making the effective area of the current emission decrease. The protrusion size can have a more profound effect on the breakdown voltages than the protrusion's aspect ratio in the cases studied. When the protrusion height is fixed, the breakdown voltage shows a minimum value as the protrusion aspect ratio increases. It has also been observed that as the aspect ratio of the microgap decreases, its influence on the breakdown voltage diminishes and saturates when $d/R \leq 1.0$. The breakdown voltage with and without the protrusion increases linearly at the same slope as the gas distance d increases. By decreasing the protrusion size, the breakdown voltage increases with a larger slope as the effective distance d_{eff} increases. This study elucidates the gas breakdown in a microdischarge with a surface protrusion and provides insights to system variability due to inherent or usage induced roughness, which might also be strategic to pre-roughen surfaces to values expected during use to reduce system variability. Future work includes the consideration of ionization distribution in the domain to further understand the non-monotonic breakdown behavior, the non-local kinetic treatment of electrons to more accurately describe the discharge,[36,37] and the modified Paschen's curve with the perturbation of surface protrusion.

The work was supported by the Air Force Office of Scientific Research (AFOSR) and the DOE Plasma Science Center Grant No. DE-SC0001939. Peng Zhang was supported by AFOSR YIP Award No. FA9550-18-1-0061.

[1]A. M. Loveless and A. L. Garner, Appl. Phys. Lett. **108**, 234103 (2016).
[2]A. Semnani, A. Venkattraman, A. A. Alexeenko, and D. Peroulis, Appl. Phys. Lett. **102**, 174102 (2013).

[3]J. P. Boeuf, L. C. Pitchford, and K. H. Schoenbach, Appl. Phys. Lett. **86**, 071501 (2005).
[4]K. H. Becker, K. H. Schoenbach, and J. G. Eden, J. Phys. D: Appl. Phys. **39**, R55 (2006).
[5]D. Mariotti and R. M. Sankaran, J. Phys. D: Appl. Phys. **43**, 323001 (2010).
[6]N. Bhattacharjee, A. Urrios, S. Kang, and A. Folch, Lab Chip **16**, 1720 (2016).
[7]S. Martínez-Jarquín, A. Moreno-Pedraza, H. Guillén-Alonso, and R. Winkler, Anal. Chem. **88**, 6976 (2016).
[8]A. M. Loveless and A. L. Garner, IEEE Trans. Plasma Sci. **45**, 574 (2017).
[9]T. Shao, W. Yang, C. Zhang, Z. Niu, P. Yan, and E. Schamiloglu, Appl. Phys. Lett. **105**, 071607 (2014).
[10]A. Venkattraman, J. Phys. D: Appl. Phys. **47**, 425205 (2014).
[11]A. Venkattraman and A. A. Alexeenko, Phys. Plasmas **19**, 123515 (2012).
[12]D. Levko and L. L. Raja, J. Appl. Phys. **117**, 173303 (2015).
[13]A. Venkattraman, A. Garg, D. Peroulis, and A. A. Alexeenko, Appl. Phys. Lett. **100**, 083503 (2012).
[14]D. B. Go and A. Venkattraman, J. Phys. D: Appl. Phys. **47**, 503001 (2014).
[15]J. A. Buendia and A. Venkattraman, EPL (Europhys. Lett.) **112**, 55002 (2015).
[16]M. A. Bilici, J. R. Haase, C. R. Boyle, D. B. Go, and R. M. Sankaran, J. Appl. Phys. **119**, 223301 (2016).
[17]Y. Feng and J. P. Verboncoeur, Phys. Plasmas **13**, 073105 (2006).
[18]S. Sun and L. K. Ang, J. Appl. Phys. **113**, 144902 (2013).
[19]Y. Feng, J. P. Verboncoeur, and M. C. Lin, Phys. Plasmas **15**, 043301 (2008).
[20]J. Lin, P. Y. Wong, P. Yang, Y. Y. Lau, W. Tang, and P. Zhang, J. Appl. Phys. **121**, 244301 (2017).
[21]P. Zhang, A. Valfells, L. K. Ang, J. W. Luginsland, and Y. Y. Lau, Appl. Phys. Rev. **4**, 011304 (2017).
[22]D. Levko and L. L. Raja, Phys. Plasmas **23**, 073513 (2016).
[23]P. Zhang, Y. Y. Lau, and R. M. Gilgenbach, J. Appl. Phys. **105**, 114908 (2009).
[24]Y. Fu, P. Zhang, J. P. Verboncoeur, A. J. Christlieb, and X. Wang, Phys. Plasmas **25**, 013530 (2018).
[25]E. A. Bogdanov, V. I. Demidov, A. A. Kudryavtsev, and A. I. Saifutdinov, Phys. Plasmas **22**, 024501 (2015).
[26]T. Farouk, B. Farouk1, D. Staack, A. Gutsol, and A. Fridman, Plasma Sources Sci. Technol. **15**, 676 (2006).
[27]G. J. M. Hagelaar and L. C. Pitchford, Plasma Sources Sci. Technol. **14**, 722 (2005).
[28]Y. Fu, J. P. Verboncoeur, and A. J. Christlieb, Phys. Plasmas **24**, 103514 (2017).
[29]Y. Fu, H. Luo, X. Zou, and X. Wang, Plasma Sources Sci. Technol. **23**, 065035 (2014).
[30]A. Derzsi, I. Korolov, E. Schüngel, Z. Donkó, and J. Schulze, Plasma Sources Sci. Technol. **24**, 034002 (2015).
[31]A. Berkane, S. Rebiai, F. Bouanaka, and H. Bahouh, Phys. Scr. **90**, 065602 (2015).
[32]J. T. Gudmundsson and A. Hecimovic, Plasma Sources Sci. Technol. **26**, 123001 (2017).
[33]J. S. Townsend, *Electricity in Gases* (Clarendon Press, Oxford, 1915).
[34]V. A. Lisovskiy, S. D. Yakovin, and V. D. Yegorenkov, J. Phys. D: Appl. Phys. **33**, 2722 (2000).
[35]Y. P. Raizer, *Gas Discharge Physics* (Springer, Berlin, 1991).
[36]A. K. Verma, A. Alamatsaz, and A. Venkattraman, J. Phys. D: Appl. Phys. **50**, 424005 (2017).
[37]R. R. Arslanbekov and V. I. Kolobov, J. Phys. D: Appl. Phys. **36**, 2986 (2003).